Featured in Physics

Quantitative feasibility study of sequential neutron captures using intense lasers

Vojtěch Horný [1,2,3,4,*] Sophia N. Chen,[4] Xavier Davoine,[2,3] Laurent Gremillet [2,3] and Julien Fuchs [1]

[1]*LULI - CNRS, École Polytechnique, CEA, Université Paris-Saclay, UPMC Université Paris 06, Sorbonne Université, F-91128, Palaiseau Cedex, France*

[2]*CEA, DAM, DIF, F-91297 Arpajon, France*

[3]*Université Paris-Saclay, CEA, LMCE, 91680 Bruyères-le-Châtel, France*

[4]*Extreme Light Infrastructure - Nuclear Physics, Horia Hulubei National Institute for Physics and Nuclear Engineering, 30 Reactorului Street, RO-077125 Bucharest-Magurele, Romania*

(Received 12 April 2023; revised 9 October 2023; accepted 21 December 2023; published 14 February 2024)

Deciphering the conditions under which neutron captures occur in the Universe to synthesize heavy elements is an endeavor pursued since the 1950s, but has proved elusive up to now due to the experimental difficulty of generating the extreme neutron fluxes required. It has been evoked that laser-driven (pulsed) neutron sources could produce neutron beams with characteristics suitable to achieve nucleosynthesis in the laboratory. In this scheme, the laser first generates an ultra-high-current, high-energy proton beam, which is subsequently converted into a dense neutron beam. Here we model, in a self-consistent manner, the transport of laser-accelerated protons through the neutron converter, the subsequent neutron generation and propagation, and finally the neutron capture reactions in gold (^{197}Au), chosen as an illustrative example. Using the parameters of present-day available lasers, as well as of those foreseeable in the near future, we find that the final yield of the isotopes containing two more neutrons than the seed nuclei is negligible. Our investigation highlights that the areal density of the laser-driven neutron source is a critical quantity and that it would have to be increased by several orders of magnitude over the current state of the art in order to offer realistic prospects for laser-based generation of neutron-rich isotopes.

DOI: 10.1103/PhysRevC.109.025802

I. INTRODUCTION

The development of high-flux neutron sources driven by ultraintense and ultrashort laser pulses has been a very active area of research over the past decade [1–3]. This interest is prompted by the unique properties of these sources compared to those produced by larger-scale nuclear fission reactors or accelerator-based spallation facilities [4,5]. In fact, the latter conventional sources are already outperformed by laser-based neutron pulses in terms of short duration, small size, and huge instantaneous flux [6]. Thanks to such features, promising applications in nondestructive and isotope-sensitive material analysis have recently been demonstrated [7].

Another potentially attractive use of laser-driven, pulsed neutron beams that have been devised in the last few years [8,9] would be to create neutron-rich isotopes, complementing traditional methods using nuclear reactors [10,11]. It was anticipated [8] that a specific benefit of such bright pulsed sources would represent an advance in laboratory astrophysics, potentially deepening our knowledge of the nucleosynthesis of elements heavier than iron.

In astrophysics, the creation of elements beyond iron is explained by slow and rapid neutron captures: the so-called *s*-process and *r*-process, respectively. In the *s*-process [12], a seed nucleus captures a neutron, resulting in the formation of an isotope with an increased atomic mass. This is followed by a β^--decay process, during which an electron and an electron antineutrino are emitted, transforming the nucleus into a higher-Z nuclide. The *s*-process is characterized by its repeated occurrence during the star's lifetime, gradually producing heavier elements. In particular, this reaction sequence encounters critical junctures, known as branching points, which determine the pathway for isotopic evolution, with some isotopes undergoing neutron capture and others electron capture, thereby influencing the final elemental composition. Ultimately, the *s*-process terminates with the isotope ^{209}Bi. Beyond this point, the subsequent neutron-capture product, ^{210}Po, is subject to α-decay, hence reducing the atomic number by two and cycling the element back to ^{206}Pb.

The origin of about half of the elements heavier than iron and all of the elements heavier than bismuth is ascribed to the *r*-process, through which sequential neutron captures drive the nuclides away from the valley of stability, in the vicinity of the neutron drip line, until an equilibrium between neutron capture and photodissociation is reached [13]. β-decays then occur, increasing the nucleus charge and allowing further neutron capture. This scenario is believed to be responsible for the synthesis of neutron-rich stable isotopes of heavy elements. To be effective, though, the *r*-process requires that extreme neutron density condition ($>10^{20}$ cm^{-3}) be attained, such as those envisioned in core-collapse supernovae [14] or neutron star mergers [15]. An intermediate or *i*-process is also thought to operate at lower neutron densities, i.e., ranging from 10^{12} to 10^{16} cm^{-3} [16,17].

*vojtech.horny@eli-np.ro

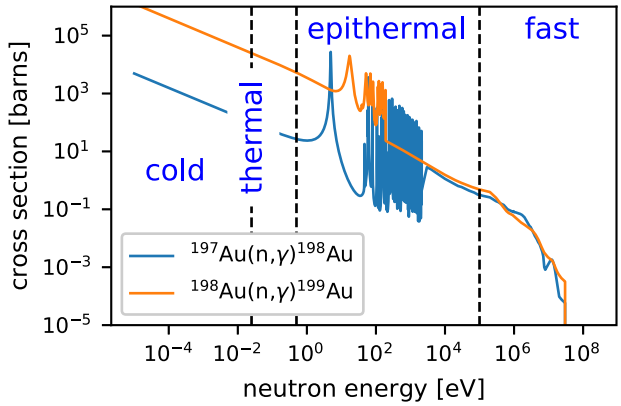

FIG. 1. Neutron capture cross section dependence on energy for ^{197}Au and ^{198}Au isotopes, from the TENDL-2019 library [24].

On Earth, the examination of the byproducts of thermonuclear explosions [18,19], during which similarly extreme neutron fluxes could be achieved, demonstrated the effectiveness of the *r*-process in producing superheavy elements. A theoretical reexamination of these results [20] concluded that a measurable amount of neutron-rich, long-lived superheavy nuclei may be synthesized employing *next-generation* pulsed reactors. In the same work [20], the requirements to be met in order to produce long-lived, superheavy elements were derived and a theoretical model was proposed to calculate the final isotope abundances.

In this paper, we quantitatively evaluate the possibility of producing neutron-rich isotopes via sequential neutron captures using pulsed neutron sources accessible to both present-day and upcoming ultrahigh-intensity ($>10^{20}$ W cm^{-2}), short-pulse (fs-ps) lasers [1,3,21,22], as discussed in Sec. II. Our study relies on a slightly modified version of the model developed in Refs. [9,20], as detailed in Sec. III and the Appendix. Calculations of the isotope yields achievable by contemporary laser-plasma sources are presented in Sec. IV. The limitations of our approach are discussed in Sec. V, and Sec. VI summarizes the study.

II. CONTEMPORARY LASER-BASED NEUTRON SOURCES

Neutrons are generally categorized in terms of energy as fast (>100 keV), epithermal (0.5 eV – 100 keV), thermal (25 meV), and cold ($\leqslant$ 25 meV) [23]. The probability of neutron capture strongly depends on the individual neutron energy; its cross-section typically grows as the neutron energy decreases, as shown in Fig. 1 for ^{197}Au, our reference material. The plotted cross sections are taken from the TENDL-2019 database [24] which collects the outputs of the TALYS nuclear model code [25]. Such an approach is necessary because measured data on neutron captures remain scarce, especially for unstable neutron-rich isotopes.

Neutron generation using intense lasers can proceed through several pathways: (p, n) or (d, n) reactions induced by the laser-accelerated protons or deuterons on light nuclei [1], spallation of heavy nuclei by hundreds-of-MeV-class protons [6], photonuclear reactions initiated by Bremsstrahlung photons generated by the accelerated electrons [2], or nuclear fission processes [26]. The flux might be further enhanced, to a certain extent, by the $(n, 2n)$ reaction [27]. In the following, we will recall the characteristics and performances of the two main types of neutron sources based on laser-plasma interactions. The moderation of the energy of the generated neutrons will also be discussed.

(a) Neutron sources driven by laser-accelerated fast ions. The most common method for generating neutrons with an intense laser pulse involves high-energy electron [2,3] or ion [1] beams accelerated from solid or foam targets. While the former case exploits photoreactions induced by Bremsstrahlung γ rays emitted by the electron beam, the latter relies on nuclear fusion reactions triggered by fast protons or deuterons on either light nuclei (e.g., Li or Be) [1] or heavy nuclei (e.g., Pb or Au) [22].

Experimentally, 100-J-class, picosecond-duration laser systems have proven effective in producing bright sources of neutrons. However, the higher intensity and repetition rate of upcoming multi-PW, few-femtosecond laser systems have the

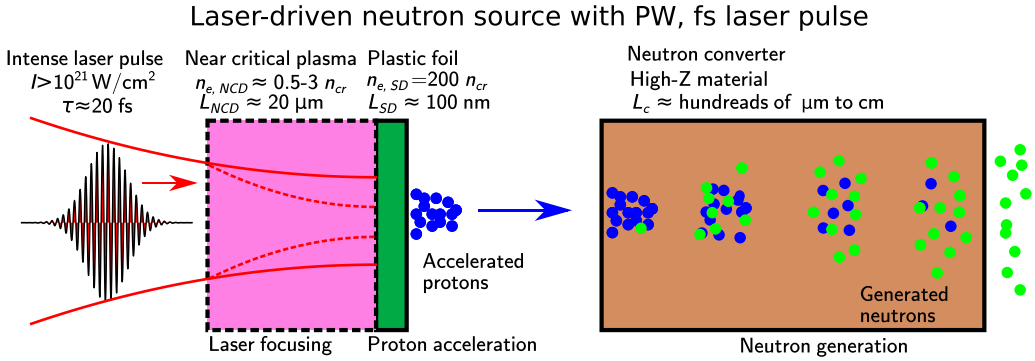

FIG. 2. Example scheme for neutron generation by a laser-driven proton beam [22]. A PW-class, ultraintense ($>10^{21}$ W cm^{-2}), ultrashort (20 fs) laser pulse interacts with a thin (submicron) solid foil (green rectangle), from which protons are accelerated. To boost the on-target laser intensity, and thus proton acceleration, a foam layer (pink box), of ≈20 μm thickness and acting, once ionized, as a near-critical-density plasma lens, can be attached to the solid foil. The neutron converter, made of a high-*Z* material (the brown box), is placed behind the laser target.

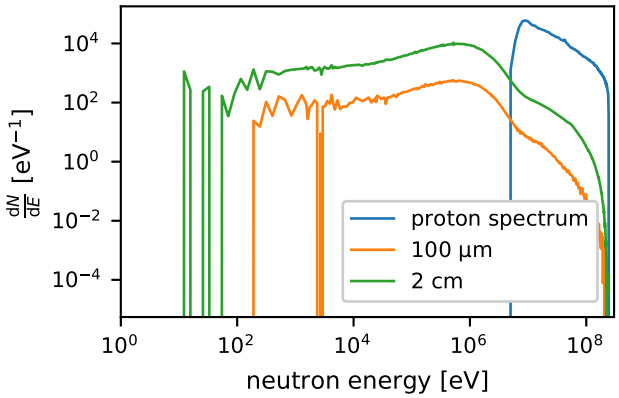

FIG. 3. Simulated neutron energy spectra (in orange and green) for the scheme shown in Fig. 2, using a 1 PW, 2×10^{21} cm^{-2}, 20 fs laser pulse, according to Ref. [22]. Neutrons are generated in a Pb converter by protons (blue spectrum) accelerated from a double-layer target, composed of a 20 μm thick, $1n_c$ density carbon layer followed by a 115 nm thick, $200n_c$ density CH_2 foil. The neutron converter has a thickness of either 100 μm (orange) or 2 cm (green).

potential to enhance proton acceleration to energies over 100 MeV, where the efficiency of the spallation process in high-Z nuclei drastically increases [6]. Such a configuration, which is considered in the following numerical study, is schematically shown in Fig. 2.

Figure 3 displays typical proton (blue) and neutron (orange, green) energy spectra, as simulated using the setup of Fig. 2. The laser-induced proton acceleration is described in 2D3V geometry (two dimensions in space, three dimensions in velocity/momentum) with the particle-in-cell CALDER code [28]. The shown proton spectrum is that obtained from a double-layer target (a carbon plasma layer of 20 μm thickness and $1n_c$ density, attached to a 115 nm, $200n_c$ CH_2 foil) [22] irradiated by a 1 PW, 2×10^{21} cm^{-2}, 20 fs laser pulse. Neutron generation in the Pb converter (of variable thickness L_c) is treated by the Monte Carlo FLUKA code [29,30].

The orange curve corresponds to a $L_c = 100$ μm thick Pb converter: while yielding the highest peak neutron intensity (i.e., exceeding 10^{23} n cm^{-2}s^{-1}), this case generates only 7.6×10^8 neutrons and an on-axis flux of 8.6×10^6 n sr^{-1} [22]. For the same input proton spectrum, the neutron flux is maximized with a $L_c = 2$ cm converter: it then reaches a value of 7.5×10^9 n sr^{-1}, for a total number of 2.4×10^{10} neutrons (see the green curve in Fig. 3). Considering a laser repetition rate of one shot per minute, this would translate into an averaged neutron flux of $\approx 10^8$ n sr^{-1} [22].

Table I presents the number of neutrons produced in various energy bands for the two considered converter thicknesses. One can see that most of the neutrons are emitted at high energies (0.1–10 MeV). It has also been found that the fastest neutrons (≈10–100 MeV) are directional, with an angular divergence decreasing with increasing energy, whereas neutrons below ≈1 MeV have a more or less isotropic distribution [22]. The downside of such a high mean neutron energy is a weak cross section of neutron capture by ^{197}Au atoms, i.e., of the order of 0.1 b (in ^{197}Au) or even lower (see Fig. 1). The potential of generating neutron-rich isotopes using this kind of neutron source is discussed in Sec. IV.

TABLE I. Number of neutrons generated in various energy bands, as computed from the neutron spectra of Fig. 3, obtained from Pb converters of two different thicknesses.

L_c	100 μm	2 cm
1 eV – 1 keV	5.96×10^4	7.64×10^5
1 keV – 10 keV	6.36×10^5	1.16×10^7
10 keV – 100 keV	1.20×10^7	2.10×10^8
100 keV – 1 MeV	4.38×10^8	7.76×10^9
1 MeV – 10 MeV	6.64×10^8	1.29×10^{10}
>10 MeV	8.67×10^7	2.67×10^9

(b) Laser-driven thermonuclear sources. Still using ultrahigh power, short laser pulses, an alternative approach to generate neutrons is to exploit thermonuclear reactions in laser-heated deuterated plasmas. Numerical simulations of the interaction of 500 J, 100 fs laser pulses focused at a moderate intensity of 10^{18} W cm^{-2} on 1 μm thick solid CD_2 foils [31] suggest that about 10^9 neutrons can be generated per laser shot, having a Gaussian spectrum with ∼2.5 MeV mean energy and ≈0.1 MeV energy spread. The angular distribution of such a source is isotropic and characterized by a $\approx 10^7$ n sr^{-1} flux per shot. These numbers are one or two orders of magnitude lower than those obtained using the above ion-beam-induced sources.

On a similar scale, $\approx 3.5 \times 10^9$ thermonuclear neutrons have been reported from laser-driven, spherically convergent plasmas with a ns, kJ-class laser [32]. Higher-flux neutron pulses can, of course, be achieved in inertial fusion implosions at MJ-class facilities. The current published record from the National Ignition Facility (NIF) is a total neutron yield of $\approx 2 \times 10^{16}$ neutrons [33], associated with a $\approx 1.6 \times 10^{15}$ n sr^{-1} flux per shot which can be repeated once per day. However, the scale, purpose, and repetition rate of those devices are obviously inadequate for any credible application related to neutron science.

(c) Moderation. All the aforementioned sources deliver fast neutrons (see Fig. 3), yet for some applications it may be desirable to decelerate them to lower energies using a moderator. This is done via successive elastic and inelastic collisions where energy exchanges between the neutrons and the moderating medium are dependent on the scattering angle. The materials used for this purpose are usually selected based on their moderating power, which is determined by the average logarithmic energy loss and the macroscopic scattering cross section [34]. A high moderation efficiency necessitates not only a high moderating power but also a weak neutron absorption. For this reason, hydrogen-based moderators (e.g., H_2, CH_4) are generally favored. To slow the neutrons down to epithermal energies, H_2O, D_2O or high-density polyethylene moderators can be employed [35]. Recently, moderation of laser-generated neutrons down to the cold energy range has been demonstrated via a staged scheme comprising a polyethylene premoderator and a cryogenic H_2 main moderator [36].

III. MODELING METHOD

We now consider the irradiation of a sample of stable seed nuclei (of mass number A) by a short neutron pulse. The final relative abundances b_i of the $(A+i)$ isotopes can be estimated using the following formulas [8,9,20] (see also the Appendix):

$$b_1 = \frac{N_1}{N_0^0} = \mu_1 \exp(-\mu_1) \simeq \mu_1, \tag{1}$$

$$b_2 = \frac{N_2}{N_0^0} = \frac{\mu_1\mu_2}{2} \exp(-\mu_2) \simeq \frac{\mu_1\mu_2}{2}, \tag{2}$$

where

$$\mu_i = \frac{dN_n}{dS}\sigma_i. \tag{3}$$

We have introduced dN_n/dS the areal density of the neutron flux, σ_i the cross section of neutron capture by the $(A+i-1)$ isotope, N_0^0 the initial number of seed nuclei, and N_i the final number of $(A+i)$ isotopes.

We now generalize this calculation to the case of a space-dependent, energy-distributed neutron flux [as in Eqs. (1) and (2), the neutron flux is too short for the temporal dependence to play a role]. Taking account of the energy dependence of σ_i, and assuming axisymmetry, the spatial map of $\mu_i(x,r)$ is then given by

$$\mu_i(x,r) = \int \frac{d^2N_n}{dS\,dE}(x,r,E)\sigma_i(E)\,dE. \tag{4}$$

There follows the total number of $(A+i)$ isotopes:

$$N_i = \frac{\rho}{Am_p}\iint b_i(x,r)\,2\pi r\,dr\,dx, \tag{5}$$

where ρ is the mass density of the seed nuclei and m_p is the proton mass. Hence, the abundance of the $(A+2)$ isotopes strongly increases as the neutron areal density grows and the neutron energy decreases (see Fig. 1).

To validate our numerical resolution of the above equations, we have reproduced the calculation of Ref. [9], i.e., using a collimated, 5 μm diameter, uniform cylindrical beam of $N_n = 10^{12}$ neutrons, with a Gaussian energy spectrum of 0.1 MeV central energy and 10% relative width. For a 100 μm thick ^{176}Lu target, we have obtained $N_1 \simeq 2.96\times10^8$ and $N_2 \simeq 615$, consistent with the results of [9].

We will now consider a more realistic space-energy-distributed neutron flux based on 3D Monte Carlo FLUKA simulations, as sketched in Fig. 4. The protons injected into the ^{197}Au material are either taken in the form of a uniform cylindrical beam with no initial divergence or extracted from the optimal particle-in-cell (PIC simulation) case #3 from [22]. The latter describes a 2×10^{21} W cm^{-2} peak intensity, 20 fs FWHM duration, 5 μm FWHM diameter laser pulse hitting at normal incidence a double-layer target composed of a 20.5 μm thick, near-critical ($n_e = 1.05n_c$) carbon layer attached to a 115 nm thick CH_2 foil ($n_e = 200n_c$). A virtual detector is placed ≈26 μm behind the rear side of the target. A total of ≈1.5×10^{12} protons are collected (the time of arrival, transverse position, and 3D momentum of each of them being recorded), characterized by an exponentially decreasing energy spectrum, extending to ≈240 MeV. A module was added

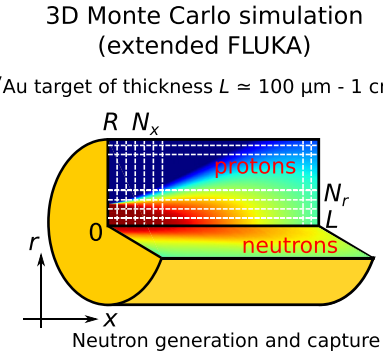

FIG. 4. Setup of Monte Carlo simulations of proton transport, neutron generation, and neutron transport. The protons are injected through the left-hand side of the ^{197}Au target. The spatial grid over which neutron captures are computed is shown as white dashed lines.

to the standard version of FLUKA to use as input the PIC proton distribution.

The target is a ^{197}Au cylinder of length L (along the x axis) and radius R. The computational grid over which the neutron flux $d^2N_n(x,r,E)/dSdE$ is discretized consists of N_r equidistant shells (along r) and N_x (along x) equidistant planes. The neutron energy, resolved by a two-way fluence (see the USRBDX entry in the FLUKA documentation [29]), is tracked across all the interfaces between the grid cells and also between the outer grid cells and vacuum.

IV. NUMERICAL RESULTS

To maximize the $(A+2)$ isotope generation rate, which scales as the square of the neutron areal density, it is preferable that the stages of neutron generation and neutron captures take place within the same target. This configuration is particularly favourable when using PW, fs-class laser systems, because the resultant >100 MeV proton beams can enable efficient neutron generation in high-Z materials [6] in which neutron captures are also the most efficient. This single-target approach allows the effective neutron areal density to be significantly enhanced in the neutron-capture material. It contrasts with present-day experiments [1,21,36] where neutrons are generated in cm-scale Be or Li converters, entailing a sizable drop in neutron fluence on the neutron-capture material located downstream. As an illustrative example, gold is here chosen to make up this multipurpose target: not only is it a sufficiently high-Z material for neutron generation to be efficient, but is also abundant and has only one stable isotope ^{197}Au.

In the following, we estimate the total neutron-rich isotope yield for various parameters of the accelerated protons or moderated neutrons that are injected into the neutron capture target. Seven configurations are considered as summarized in Table II. Six of them (cases A–F) represent idealized sources of laser-accelerated protons, taken to be perfectly collimated, monoenergetic (with energies ranging from 20 MeV and 1 GeV) and with a uniform cylindrical profile of 25 μm^2 cross-sectional area. Based on Ref. [9], the number of incident protons is set to 10^{12}, yielding an areal density of

TABLE II. Parameters of the neutron-capture calculations: E, S, and N are the energy, cross-sectional area, and particle number characterizing the proton source, R and L are the radius and length of the neutron-capture ^{197}Au target, and N_1 and N_2 denote the ^{198}Au and ^{199}Au yields. Cases A–F consider a monoenergetic, cylindrical proton beam while case G uses the proton distribution extracted from PIC simulation #3 in [22]. The values of R and L are chosen so as to accommodate the production of the vast majority of isotopes using a reasonable grid resolution, with the constraint that the number of internal detectors in FLUKA cannot exceed 1100 [37].

	E	S	N	R	L	N_1	N_2
A	20 MeV	25 μm^2	10^{12}	20 μm	0.5 mm	3.2×10^4	3.5×10^{-8}
B	50 MeV	25 μm^2	10^{12}	20 μm	0.5 mm	1.5×10^5	4.5×10^{-7}
C	100 MeV	25 μm^2	10^{12}	20 μm	0.5 mm	1.8×10^5	7.3×10^{-7}
D	200 MeV	25 μm^2	10^{12}	15 μm	0.75 mm	2.4×10^5	1.0×10^{-6}
E	500 MeV	25 μm^2	10^{12}	15 μm	1.0 mm	3.4×10^5	2.0×10^{-6}
F	1 GeV	25 μm^2	10^{12}	15 μm	1.0 mm	4.0×10^5	2.9×10^{-6}
G	as case #3 in [22]		1.5×10^{12}	250 μm	0.3 mm	4.7×10^5	8.5×10^{-8}

4×10^{18} $p\,\mathrm{cm}^{-2}$ at the target front side. The target parameters R and L (see Table II) are chosen such that the volume where neutron captures mainly occur is properly resolved.

The left column of Fig. 5 [panels (a), (c), (e), (g)] details the results obtained in case C, where a narrow beam of collimated 100 MeV protons is used as input (see Table II). Figure 5(a) visualizes the transport of the proton beam through the target. A steady decrease in the proton areal density is apparent: after 500 μm of propagation, the on-axis proton areal density drops to 2.9×10^{17} $p\,\mathrm{cm}^{-2}$, mainly as a result of elastic collisions, and, to a lesser degree, absorption. Panel (c) shows the corresponding neutron areal density. Its on-axis areal density reaches a maximum of 1.20×10^{15} $n\,\mathrm{cm}^{-2}$ at $x_{\max} \simeq 54$ μm, and decreases deeper into the target, although the total number of neutrons reaching a position $x > x_{\max}$ keeps on growing with $x < L$. This behavior arises from the increasingly divergent proton beam caused by scattering within the target. Panels (e) and (g) show the predicted abundance maps of the ^{198}Au and ^{199}Au isotopes, the total numbers of which are given in Table II. While the ^{198}Au yield per laser shot ($N_1 = 1.8 \times 10^5$) could be easily measured experimentally, the ^{199}Au yield ($N_2 = 7.3 \times 10^{-7}$) is much too low to be detected, even by accumulating a large number of shots, as would be allowed, in principle, by the 3-day half-lives of ^{198}Au and ^{199}Au. The other idealized configurations do not provide any significant progress in this regard.

The right column of Fig. 5 shows the results of case G, where use is made of the proton beam predicted from PIC simulation #3 in [22], as detailed above. Panel (b) indicates that this more realistic source, which covers a transverse area of a few 100 μm^2, is characterized by a maximum areal density of $\approx 1.1 \times 10^{17}$ $p\,\mathrm{cm}^{-2}$ and is rather divergent with a peak at $\approx 17^\circ$ relative to the x axis. Panel (d) shows that the neutrons are preferentially emitted along this direction, yet their angular distribution is not as peaked as that of the protons. A relatively high number of neutrons are produced around the x axis, even though the proton density is quite low there. The explanation is that the fastest protons are injected at small angles, as seen in the energy-angle ion spectrum shown in the inset of panel (b). Panels (f) and (h) show that the $(A+1)$ and $(A+2)$ isotopes are created over a much larger transverse area than in case C. The total yield of ^{198}Au isotopes ($N_1 \simeq 4.5 \times 10^5$) exceeds that achieved in cases A–F. By contrast, however, only 8.5×10^{-8} ^{199}Au isotopes are produced in total (see Table II). This seemingly contradictory result is explained by the different scalings of the isotope abundances b_i with the neutron areal density: b_1 scales as $b_1 \propto dN_n/dS$ whereas $b_2 \propto (dN_n/dS)^2$.

For all considered cases, the total number of generated ^{199}Au nuclei is at best of the order of 10^{-6} per shot, or even less. Hence, we can conclude that sequential neutron captures cannot be experimentally detected, and this even under the unrealistically extreme conditions of cases A–F, which indeed seem out of reach even of future 10 PW laser systems. Considering that a minimum number of about 10^{4-5} of isotopes per shot is necessary for their detection, contemporary short-pulse laser-driven neutron sources appear clearly unsuited to laboratory investigations of $(A+2)$ isotope generation or r-process nucleosynthesis, at least for the irradiation setups considered up to now. However, we will see in the following discussion that thermalization of laser-driven neutrons to cryogenic temperatures, as already demonstrated experimentally [36], may generate detectable amounts of $(A+2)$ isotopes, provided that the driving PW-class lasers can operate at a high enough ($\approx$100 Hz) repetition rate. Although not currently available, such a capability can be envisioned in the relatively near future [38–40].

V. DISCUSSION

First, let us point out that the generation of neutron-rich isotopes can be increased by using moderators. As Eq. (2) suggests, the final abundance of the $(A+2)$ isotope after a certain neutron exposure scales as $\sim \sigma_1 \sigma_2 N_n^2/S$. Hence, neutron moderation results in two opposing effects: (1) the neutron-capture cross section significantly grows, and (2) the neutron flux considerably decreases due to geometrical reasons and absorption. The former may be greatly beneficial for the production of neutron-rich isotopes.

In the following paragraphs, we examine whether a moderated neutron source driven by a short-pulse laser could be employed for generating of $(A+2)$th isotopes and how demanding it would be. To this goal, we consider the parameters of the cold neutron source recently reported in Ref. [36]. In that experiment, a 300 J, 1.2 ps laser pulse was employed to generate fast protons (up to $\approx$5 MeV) and deuterons (up to

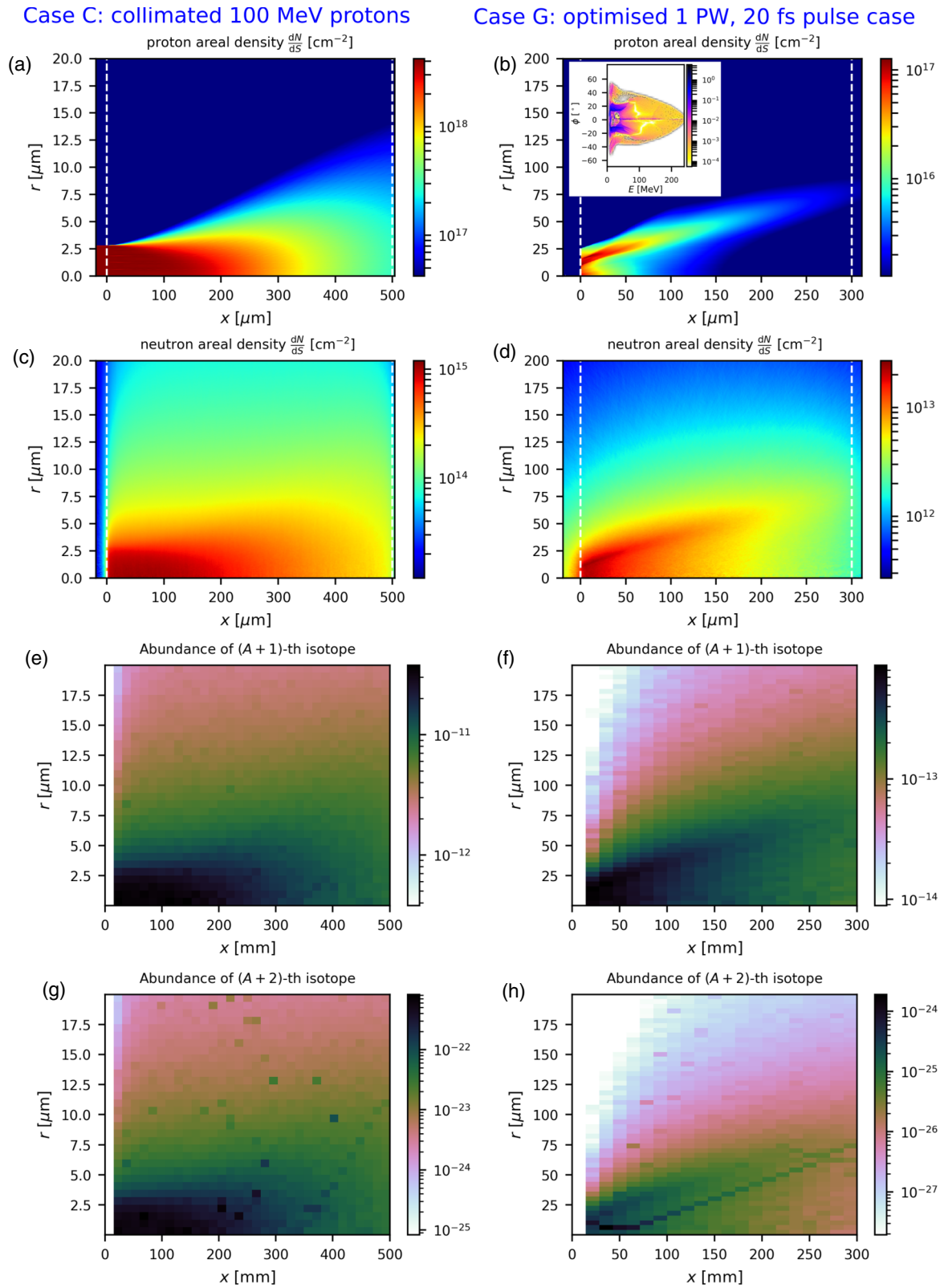

FIG. 5. Proton [(a), (b)] and neutron [(c), (d)] transport through the ^{197}Au converter (located between the two white dashed lines) and final abundances of ^{198}Au [(e), (f)] and ^{199}Au [(g), (h)] for cases C [(a), (c), (e), (g)] and G from Table II, respectively. The inset in panel (b) displays the energy-angle spectrum of the incident protons in case G.

≈20 MeV) from a 5 μm thick deuterated polyethylene (C_2D_4) target via target normal sheath acceleration. Those ions were subsequently converted into neutrons in a cm-scale Be target, yielding a fast neutron flux of $\approx 10^9$ $n\,\mathrm{sr}^{-1}$, quite similar to case G considered above. These fast neutrons were then slowed down through an off-axis, wing-shaped (10 mm × 6 mm × 5 mm) polyethylene premoderator attached to the converter and a cryogenically cooled H_2 gas serving as the main moderator. The 27 nm thick moderator was placed within a 2 mm thick container made of copper. As a result, $\approx 10^7$ cold neutrons were released per shot, associated with a $\approx 4 \times 10^5$ cm^{-2} areal density at the surface of the H_2 moderator. In the discussion section of [36], the authors mention that their upgraded laser system could ultimately work at 100 Hz repetition rate. Considering eight hours of uninterrupted operation, the total integrated cold neutron areal density at the converter surface could be as high as 10^{12} cm^{-2}.

We address the same configuration, but in which the container of the cryogenic H_2 gas is made of gold instead of copper. For simplicity, we further assume that the container is spherical with 27 mm diameter and 2 mm thickness [23]. Taking the cold neutron energy distribution to be Gaussian with central energy of 20 meV, a relative energy spread of 10% and the aforementioned available areal density of 4×10^5 cm^{-2}, we can estimate that the numbers of generated ^{198}Au and ^{199}Au would be $N_1 = 3.8 \times 10^{13}$ and $N_2 = 5.3 \times 10^5$, respectively, thus making the latter detectable. We can conclude that while it is, in principle, possible to use a short-pulse laser-driven neutron source to generate $(A+2)$ isotopes, the setup involved would not bring any advantage over small, easy-to-handle gold foils at a research reactor.

Regarding the discrepancy between our estimates and the much higher isotope yield predicted in Refs. [8,9], we first point out the greater accuracy of our modeling approach. Not only is it based on state-of-the-art Monte Carlo simulations of the proton transport, neutron generation, and propagation in the target serving both as neutron converter and neutron capture target, but it also considers a realistic input source of protons as predicted by an optimized PIC simulation. The difference between our results and those of Refs. [8,9] stems chiefly from the characteristics of the neutron pulse used to induce isotope generation. The areal density ($dN_n/dS \simeq 4 \times 10^{18}$ $n\,\mathrm{cm}^{-2}$) of the perfectly collimated neutron source considered in Ref. [9] turns out to overestimate that of laser-driven neutrons by orders of magnitude. For instance, when taking account of a realistic proton source for a 1 PW, 20 fs laser system as is done in case G above, our approach predicts $dN_n/dS \simeq 2 \times 10^{13}$ $n\,\mathrm{cm}^{-2}$. Moreover, the energy spectrum of the supposedly laser-driven source in [9] is taken to be Gaussian with a mean energy between 50 keV and 10 MeV and a relative width of 10%. Such parameters are at odds with previous experimental findings [1,3,23,41] and our own results, which show much broader neutron spectra.

Similarly, we should mention that the production of $(A+2)$ isotopes was considerably overestimated in [8] due to the erroneous assumption that the cross section of neutron capture keeps a constant value of 1 b at all neutron energies. This error stemmed from the fact that the total cross section for all reactions involving neutrons is flat; yet this does not hold when considering only multiple neutron captures, in which case the cross section indeed drops quickly with neutron energy. This caused the cross section to be overestimated by one to three orders of magnitude for 100 keV – 10 MeV neutrons, and even more for faster neutrons. This paper, however, considered a neutron flux of 10^{24} $n\,\mathrm{cm}^{-2}\,\mathrm{s}^{-1}$ and 1 ns duration, corresponding to an areal density of $\approx 10^{13}$ $n\,\mathrm{cm}^{-2}$, similar to that characterizing our case G. The error in the cross section led to a $(A+2)$ isotope abundance reaching 4×10^{-18}, much above that ($\simeq 2 \times 10^{-24}$) attained in case G; see Fig. 5(h).

Finally, one important aspect is the production of isotopes via *unwanted* channels. In our case, for example, when the gold itself acts as a proton-to-neutron converter, other reaction channels such as *p*-induced impurities in gold are open. As these impurities (here mainly Bi, Pb, and Tl) are likely more abundant than the freshly produced ^{199}Au, such reactions should be considered when analyzing the generation of the latter isotope.

VI. CONCLUSION

We have carried out detailed numerical computations to assess the feasibility of realizing multiple neutron captures in laser-based experiments, under conditions relevant to astrophysical nucleosynthesis. First, considering either idealized, monoenergetic and monodirectional, primary proton beams or a realistic proton distribution, as expected to be driven by a 1-PW-class short pulse laser [22], we performed Monte Carlo FLUKA simulations of the generation and transport of fast neutrons through a high-*Z* target serving both as neutron converter and neutron-capture target. ^{197}Au was chosen as an illustrative example. We then processed the resultant neutron areal density maps to compute the total yields of ^{198}Au and ^{199}Au isotopes. At variance with the encouraging conclusions reached in the recent literature [8,9], we predict that at best the negligible amount of 10^{-6} ^{199}Au isotopes can be produced per laser shot, even by resorting to overtly optimistic proton beam parameters.

We then tested whether thermalization of laser-driven neutrons to cryogenic temperatures, as recently demonstrated experimentally [36], would allow, by increasing drastically the neutron-capture cross section, a detectable number of $(A+2)$ isotopes to be produced. We estimate that this might be indeed possible provided a jump in technology is achieved, resulting in PW-class lasers operating at least at 100 Hz repetition rate. Much effort is being currently devoted to this goal worldwide, notably through diode-pumped amplification schemes [38–40,42,43].

ACKNOWLEDGMENTS

This work was supported by funding from the European Research Council (ERC) under the European Union's Horizon 2020 research and innovation program (Grant Agreement No. 787539, project GENESIS), and by Grant No. ANR-17-CE30-0026-Pinnacle from Agence Nationale de la Recherche. Extreme Light Infrastructure Nuclear Physics (ELI-NP) Phase II, is a project cofinanced by the Romanian Government and the European Union through the European

Regional Development Fund and the Competitiveness Operational Programme (1/07.07.2016, COP, ID 1334). This work was supported by the contract sponsored by the Romanian Ministry of Research and Innovation, PN 23 21 01 05, and the IOSIN funds for research infrastructures of national interest. We acknowledge GENCI-TGCC for granting us access to the supercomputer IRENE under Grants No. A0100507594 and No. A0110512993.

APPENDIX: CALCULATION OF THE ISOTOPE ABUNDANCES

The number of isotopes generated upon irradiating a thin target layer by a neutron beam containing N_n particles over an area S is given by [9]

$$\mathbf{N} = e^{\mathbf{B}}\mathbf{N_0} = \left(\sum_{k=0}^{\infty}\frac{\mathbf{B}^k}{k!}\right)\mathbf{N_0}, \tag{A1}$$

where $\mathbf{N} = (N_0, N_1, N_2, \dots)^{\mathrm{T}}$ and $\mathbf{N_0} = (N_0^0, N_1^0, N_2^0, \dots)^{\mathrm{T}}$ are the initial and final populations of the $(A+i)$ isotopes $(i = 0, 1, 2\dots)$. Furthermore, we have introduced

$$\mathbf{B} = \begin{bmatrix} -\eta_0 & 0 & 0 & \dots & 0 \\ \mu_0 & -\eta_1 & 0 & \dots & 0 \\ 0 & \mu_1 & -\eta_2 & \dots & 0 \\ \vdots & \vdots & \vdots & \ddots & \vdots \\ 0 & \dots & \dots & \mu_{l-1} & 0 \end{bmatrix}, \tag{A2}$$

$$\mu_i = \frac{N_n\sigma_{c,i}}{S}, \tag{A3}$$

$$\eta_i = \frac{N_n\sigma_{tr,i}}{S}, \tag{A4}$$

where $\sigma_{c,i}$ is the neutron-capture cross section of the $(A+i)$ isotope and $\sigma_{tr,i}$ its transmutation cross section, including all processes changing the neutron or proton number.

Considering only single and double neutron capture, we can rewrite Eq. (A1) as

$$\begin{aligned}\mathbf{N} &= \left(\mathbf{I} + \mathbf{B} + \frac{\mathbf{B}^2}{2}\right)\mathbf{N_0} \\ &= \begin{bmatrix} 1-\eta_0+\frac{\eta_0^2}{2} & 0 & 0 \\ \mu_0\left(1-\frac{\eta_0}{2}-\frac{\eta_1}{2}\right) & 1-\eta_1+\frac{\eta_1^2}{2} & 0 \\ \frac{\mu_0\mu_1}{2} & \mu_1\left(1-\frac{\eta_1}{2}\right) & 1 \end{bmatrix}\mathbf{N_0}.\end{aligned} \tag{A5}$$

Given the initial conditions $\mathbf{N_0} = (N_0^0, 0, 0)^{\mathrm{T}}$, the final populations are

$$N_0 = \left(1-\eta_0+\frac{\eta_0^2}{2}\right)N_0^0 \approx N_0^0, \tag{A6}$$

$$N_1 = \mu_0\left(1-\frac{\eta_0}{2}-\frac{\eta_1}{2}\right)N_0 \approx \mu_0 N_0, \tag{A7}$$

$$N_2 = \frac{\mu_0\mu_1}{2}N_0. \tag{A8}$$

[1] M. Roth, D. Jung, K. Falk, N. Guler, O. Deppert, M. Devlin, A. Favalli, J. Fernandez, D. Gautier, M. Geissel *et al.*, Bright laser-driven neutron source based on the relativistic transparency of solids, Phys. Rev. Lett. **110**, 044802 (2013).

[2] I. Pomerantz, E. McCary, A.R. Meadows, A. Arefiev, A.C. Bernstein, C. Chester, J. Cortez, M.E. Donovan, G. Dyer, E.W. Gaul, D. Hamilton, D. Kuk, A.C. Lestrade, C. Wang, T. Ditmire, B.M. Hegelich, Ultrashort pulsed neutron source, Phys. Rev. Lett. **113**, 184801 (2014).

[3] M. Günther, O. Rosmej, P. Tavana, M. Gyrdymov, A. Skobliakov, A. Kantsyrev, S. Zähter, N. Borisenko, A. Pukhov, and N. Andreev, Forward-looking insights in laser-generated ultra-intense γ-ray and neutron sources for nuclear application and science, Nat. Commun. **13**, 170 (2022).

[4] G. S. Bauer, Physics and technology of spallation neutron sources, Nucl. Instrum. Methods Phys. Res., Sect. A **463**, 505 (2001).

[5] D. Filges and F. Goldenbaum, *Handbook of Spallation Research: Theory, Experiments and Applications* (Wiley, New York, 2009).

[6] B. Martinez, S. Chen, S. Bolaños, N. Blanchot, G. Boutoux, W. Cayzac, C. Courtois, X. Davoine, A. Duval, V. Horny *et al.*, Numerical investigation of spallation neutrons generated from petawatt-scale laser-driven proton beams, Matter Radiat. Extremes **7**, 024401 (2022).

[7] M. Zimmer, S. Scheuren, A. Kleinschmidt, N. Mitura, A. Tebartz, G. Schaumann, T. Abel, T. Ebert, M. Hesse, Ş. Zähter, S. C. Vogel, O. Merle, R.-J. Ahlers, S. Duarte Pinto, M. Peschke, T. Kröll, V. Bagnoud, C. Rödel, and M. Roth, Demonstration of non-destructive and isotope-sensitive material analysis using a short-pulsed laser-driven epi-thermal neutron source, Nat. Commun. **13**, 1173 (2022).

[8] S. Chen, F. Negoita, K. Spohr, E. d'Humières, I. Pomerantz, and J. Fuchs, Extreme brightness laser-based neutron pulses as a pathway for investigating nucleosynthesis in the laboratory, Matter Radiat. Extremes **4**, 054402 (2019).

[9] P. Hill and Y. Wu, Exploring laser-driven neutron sources for neutron capture cascades and the production of neutron-rich isotopes, Phys. Rev. C **103**, 014602 (2021).

[10] F. F. (Russ) Knapp Jr., S. Mirzadeh, A. Beets, and M. Du, Production of therapeutic radioisotopes in the ORNL High Flux Isotope Reactor (HFIR) for applications in nuclear medicine, oncology and interventional cardiology, J. Radiat. Nucl. Chem. **263**, 503 (2005).

[11] N. Lepareur, F. Lacœuille, C. Bouvry, F. Hindré, E. Garcion, M. Chérel, N. Noiret, E. Garin, and F. R. Knapp, Jr., Rhenium-188 labeled radiopharmaceuticals: current clinical applications in oncology and promising perspectives, Front. Med. **6**, 132 (2019).

[12] E. M. Burbidge, G. R. Burbidge, W. A. Fowler, and F. Hoyle, Synthesis of the elements in stars, Rev. Mod. Phys. **29**, 547 (1957).

[13] J. J. Cowan, C. Sneden, J. E. Lawler, A. Aprahamian, M. Wiescher, K. Langanke, G. Martínez-Pinedo, and F.-K. Thielemann, Origin of the heaviest elements: The rapid neutron-capture process, Rev. Mod. Phys. **93**, 015002 (2021).

[14] S. Andrews, C. Fryer, W. Even, S. Jones, and M. Pignatari, The nucleosynthetic yields of core-collapse supernovae: Prospects for the next generation of gamma-ray astronomy, Astrophys. J. **890**, 35 (2020).

[15] D. Kasen, B. Metzger, J. Barnes, E. Quataert, and E. Ramirez-Ruiz, Origin of the heavy elements in binary neutron-star mergers from a gravitational-wave event, Nature (London) **551**, 80 (2017).

[16] J. J. Cowan and W. K. Rose, Production of ^{14}C and neutrons in red giants, Astrophys. J. **212**, 149 (1977).

[17] A. Choplin, L. Siess, and S. Goriely, The intermediate neutron capture process. I. Development of the i-process in low-metallicity low-mass AGB stars, Astronomy Astrophys. **648**, A119 (2021).

[18] H. Diamond, P. Fields, C. Stevens, M. Studier, S. Fried, M. Inghram, D. Hess, G. Pyle, J. Mech, W. Manning *et al.*, Heavy isotope abundances in Mike thermonuclear device, Phys. Rev. **119**, 2000 (1960).

[19] Y. S. Lutostansky and V. Lyashuk, Production of transuranium nuclides in pulsed neutron fluxes from thermonuclear explosions, JETP Lett. **107**, 79 (2018).

[20] V. I. Zagrebaev, A. V. Karpov, I. N. Mishustin, and W. Greiner, Production of heavy and superheavy neutron-rich nuclei in neutron capture processes, Phys. Rev. C **84**, 044617 (2011).

[21] A. Kleinschmidt, V. Bagnoud, O. Deppert, A. Favalli, S. Frydrych, J. Hornung, D. Jahn, G. Schaumann, A. Tebartz, F. Wagner *et al.*, Intense, directed neutron beams from a laser-driven neutron source at PHELIX, Phys. Plasmas **25**, 053101 (2018).

[22] V. Horný, S. N. Chen, X. Davoine, V. Lelasseux, L. Gremillet, and J. Fuchs, High-flux neutron generation by laser-accelerated ions from single-and double-layer targets, Sci. Rep. **12**, 19767 (2022).

[23] S. R. Mirfayzi, A. Alejo, H. Ahmed, D. Raspino, S. Ansell, L. A. Wilson, C. Armstrong, N. M. Butler, R. Clarke, A. Higginson *et al.*, Experimental demonstration of a compact epithermal neutron source based on a high power laser, Appl. Phys. Lett. **111**, 044101 (2017).

[24] A. Koning, D. Rochman, J.-C. Sublet, N. Dzysiuk, M. Fleming, and S. Van der Marck, TENDL: complete nuclear data library for innovative nuclear science and technology, Nucl. Data Sheets **155**, 1 (2019).

[25] A. J. Koning, S. Hilaire, and M. C. Duijvestijn, TALYS: Comprehensive nuclear reaction modeling, in *International Conference on Nuclear Data for Science and Technology*, edited by R. C. Haight, M. B. Chadwick, T. Kawano, and P. Talou, AIP Conf. Proc. No. 769 (AIP, New York, 2005), p. 1154.

[26] T. E. Cowan, A. W. Hunt, T. W. Phillips, S. C. Wilks, M. D. Perry, C. Brown, W. Fountain, S. Hatchett, J. Johnson, M.H. Key, T. Parnell, D. M. Pennington, R. A. Snavely, and Y. Takahashi, Photonuclear fission from high energy electrons from ultraintense laser-solid interactions, Phys. Rev. Lett. **84**, 903 (2000).

[27] M. Hohenberger, S. Kerr, C. Yeamans, D. Rusby, K. Meaney, K. Hahn, R. Heredia, T. Sarginson, B. Blue, A. Mackinnon *et al.*, A combined MeV-neutron and x-ray source for the National Ignition Facility, Rev. Sci. Instrum. **93**, 103510 (2022).

[28] E. Lefebvre, N. Cochet, S. Fritzler, V. Malka, M.-M. Aléonard, J.-F. Chemin, S. Darbon, L. Disdier, J. Faure, A. Fedotoff *et al.*, Electron and photon production from relativistic laser–plasma interactions, Nucl. Fusion **43**, 629 (2003).

[29] T. Böhlen, F. Cerutti, M. Chin, A. Fassò, A. Ferrari, P. G. Ortega, A. Mairani, P. R. Sala, G. Smirnov, and V. Vlachoudis, The FLUKA code: developments and challenges for high energy and medical applications, Nucl. Data Sheets **120**, 211 (2014).

[30] V. Vlachoudis *et al.*, FLAIR: a powerful but user friendly graphical interface for FLUKA, in *Proceedings of the International Conference on Mathematics, Computational Methods & Reactor Physics (M&C 2009), Saratoga Springs, NY, May 3–7, 2009* (American Nuclear Society, LaGrange Park, IL, 2009).

[31] Y. Wu, Neutron production from thermonuclear reactions in laser-generated plasmas, Phys. Plasmas **27**, 022708 (2020).

[32] G. Ren, J. Yan, J. Liu, K. Lan, Y.H. Chen, W.Y. Huo, Z. Fan, X. Zhang, J. Zheng, Z. Chen, W. Jiang, L. Chen, Q. Tang, Z. Yuan, F. Wang, S. Jiang, Y. Ding, W. Zhang, and X.T. He, Neutron generation by laser-driven spherically convergent plasma fusion, Phys. Rev. Lett. **118**, 165001 (2017).

[33] A. B. Zylstra, A. L. Kritcher, O. A. Hurricane, D. A. Callahan, K. Baker, T. Braun, D. T. Casey, D. Clark, K. Clark, T. Doppner, L. Divol, D. E. Hinkel, M. Hohenberger, C. Kong, O. L. Landen, A. Nikroo, A. Pak, P. Patel, J. E. Ralph, N. Rice, R. Tommasini, M. Schoff, M. Stadermann, D. Strozzi, C. Weber, C. Young, C. Wild, R. P. J. Town, and M. J. Edwards, Record energetics for an inertial fusion implosion at NIF, Phys. Rev. Lett. **126**, 025001 (2021).

[34] W. M. Stacey, *Nuclear Reactor Physics* (John Wiley & Sons, New York, 2018).

[35] S. Mirfayzi, H. Ahmed, D. Doria, A. Alejo, S. Ansell, R. Clarke, B. Gonzalez-Izquierdo, P. Hadjisolomou, R. Heathcote, T. Hodge *et al.*, A miniature thermal neutron source using high power lasers, Appl. Phys. Lett. **116**, 174102 (2020).

[36] S. Mirfayzi, A. Yogo, Z. Lan, T. Ishimoto, A. Iwamoto, M. Nagata, M. Nakai, Y. Arikawa, Y. Abe, D. Golovin *et al.*, Proof-of-principle experiment for laser-driven cold neutron source, Sci. Rep. **10**, 20157 (2020).

[37] G. Battistoni, T. Boehlen, F. Cerutti, P. W. Chin, L. S. Esposito, A. Fassò, A. Ferrari, A. Lechner, A. Empl, A. Mairani *et al.*, Overview of the FLUKA code, Ann. Nucl. Energy **82**, 10 (2015).

[38] E. Sistrunk, T. Spinka, A. Bayramian, S. Betts, R. Bopp, S. Buck, K. Charron, J. Cupal, R. Deri, M. Drouin, A. Erlandson, E. S. Fulkerson, J. Horner, J. Horacek, J. Jarboe, K. Kasl, D. Kim, E. Koh, L. Koubikova, R. Lanning, W. Maranville, C. Marshall, D. Mason, J. Menapace, P. Miller, P. Mazurek, A. Naylon, J. Novak, D. Peceli, P. Rosso, K. Schaffers, D. Smith, J. Stanley, R. Steele, S. Telford, J. Thoma, D. VanBlarcom, J. Weiss, P. Wegner, B. Rus, and C. Haefner, All diode-pumped, High-repetition-rate Advanced Petawatt Laser System (HAPLS), in *Conference on Lasers and Electro-Optics* (Optica, Washington, 2017), p. STh1L.2.

[39] M. Hübner, I. Will, J. Körner, J. Reiter, M. Lenski, J. Tümmler, J. Hein, B. Eppich, A. Ginolas, and P. Crump, Novel high-power, high repetition rate laser diode pump modules suitable for high-energy class laser facilities, Instruments **3**, 34 (2019).

[40] C. N. Danson, C. Haefner, J. Bromage, T. Butcher, J.-C. F. Chanteloup, E. A. Chowdhury, A. Galvanauskas, L. A. Gizzi, J. Hein, D. I. Hillier *et al.*, Petawatt and exawatt class lasers worldwide, High Power Laser Sci. Eng. **7**, e54 (2019).

[41] N. Guler, P. Volegov, A. Favalli, F. E. Merrill, K. Falk, D. Jung, J. L. Tybo, C. H. Wilde, S. Croft, C. Danly *et al.*, Neutron

imaging with the short-pulse laser driven neutron source at the Trident laser facility, J. Appl. Phys. **120**, 154901 (2016).

[42] N. Jourdain, U. Chaulagain, M. Havlík, D. Kramer, D. Kumar, I. Majerová, V. Tikhonchuk, G. Korn, and S. Weber, The L4n laser beamline of the P3-installation: Towards high-repetition rate high-energy density physics at ELI-Beamlines, Matter Radiat. Extremes **6**, 015401 (2021).

[43] A. Iwamoto and R. Kodama, Conceptual design of a subcritical research reactor for inertial fusion energy with the J-EPoCH facility, High Energy Density Phys. **36**, 100842 (2020).